JOURNAL OF SOLID STATE CHEMISTRY 62, 92–104 (1986)

The Structures of Bi_3PbWO_8Cl and Bi_4NbO_8Cl and the Evolution of the Bipox Structure Series

JOHN F. ACKERMAN

General Electric Corporate Research Development Labs, One River Road, Schenectady, New York 12301

Received August 23, 1985

A new adaptive structure series is described which is a mixture of Aurivillius phases and Sillen's phases. The structures of two of the simplest members of this series are presented.

Introduction

$[Bi_2O_2]^{2+}$ layers have been observed in two different adaptive series, the Aurivillius phases (*1*) and Sillén's phases (*2*). In the Aurivillius phases the $[Bi_2O_2]^{2+}$ layers are found between perovskitic layers of formula $[A_{n-1}M_nO_{3n+1}]^{2-}$ where n denotes the thickness of the perovskitic layers in terms of MO_6 octahedra. Thus, when $n = 1$, $[A_{n-1}M_nO_{3n+1}]^{2-} = [MO_4]^{2-}$ and the perovskitic layer is one metal–oxygen octahedron thick. Electroneutrality dictates M to be a 6+ ion; so that a stoichiometry of $[Bi_2O_2][WO_4]$ is obtained. The structure of this material, γBi_2WO_6, is shown in Fig. 1A. Similar considerations will lead to the formulas of the $n = 2$ and $n = 3$ materials, Bi_3NbTiO_9[1] and $Bi_4Ti_3O_{12}$,[1] whose structures are shown in Figs. 1B and 1C. Note that there are two perovskitic layers per cell so that an increase in the perovskitic layer by amount x increases the c axis of the cell by $2x$. Some Aurivillius phases exhibit pseudotetragonal symmetry crystallizing in orthorhombic space groups. In such materials the true axes are located 45° from the pseudotetragonal a_0 and have length $\sqrt{2}\,a_0$. A large number of Aurivillius phases have been structurally characterized and all have tetragonal or pseudotetragonal a_0 between 3.85–3.95 Å ($a_{\text{orthorhombic}}$5.45–5.58 Å). Thus the structural behavior of this series is predictable; the unit cells are tetragonal or nearly so, and for every unit increase in n there is an increase in $c_0/2$ of approximately 3.9 Å, the thickness of one metal–oxygen octahedron. Structural concepts may be developed assuming tetragonal lattices having $a_0 \simeq 3.85$ and c_0 varying.

In Sillen's phases $[Bi_2O_2]^{2+}$ and isostructural $[PbBiO_2]^{1+}$ layers are found between halogen or alkali–halogen layers of formula $[X]$, and $[AX]_2$ (X = Cl, Br, I, A = Na, K, Rb). The single and double halogen layer materials $[BiPbO_2][Cl]$ and $[Bi_2O_2][Cl][Cl]$ are shown in Figs. 2A and 2B. Again the unit cells are approximately tetragonal with $a_0 \cong 3.85$ Å and c_0 varying in a predictable manner.

The common occurrence of the $[Bi_2O_2]$

[1] A in $[A_{n-1}M_nO_{3n+1}]^{1-}$ is normally set equal to Bi^{3+} to simplify synthesis.

0022-4596/86 $3.00

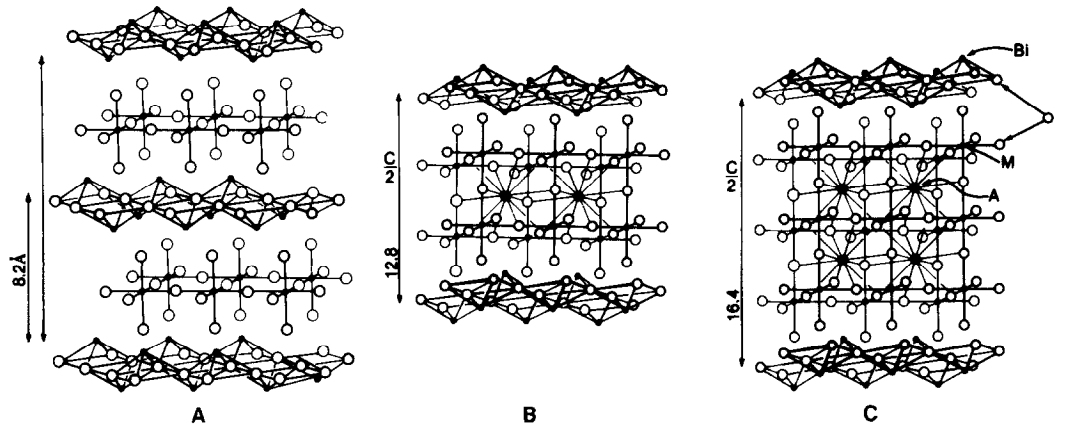

FIG. 1. Structures of Aurivillius phases: (A) $n = 1$, γBi_2WO_6, (B) $n = 2$, Bi_3NbTiO_9, (C) $n = 3$, $Bi_4Ti_3O_{12}$.

layers in these two structues together with the apparent structural integrity of the $[Bi_2O_2]$, $[A_{n-1}M_nO_{3n+1}]$, and [Cl] layers suggested that it may be possible to synthesize a new adaptive series containing all three layers in which individual layer integrity is still preserved. Stoichiometries of members of this series can be found by selecting the layers, fixing the stoichiometries of the $[Bi_2O_2]$ and halogen layers, then finding a transition metal within the perovskitic layer which satisfies electroneutrality and size constraints. For example, the simplest member of this series would have the layer composition $[Bi_2O_2]^{2+}[Cl]^-[Bi_2O_2]^{2+}[A_{n-1}M_nO_{3n+1}]^{3-}$ with $n = 1$. This reduces to $[Bi_2O_2][Cl][Bi_2O_2][MO_4]$; hence to make an electroneutral compound M must be pentavalent, producing Bi_4NbO_8Cl.

Written in this fashion it is easy to conceptualize the structure of this compound as being a 1+ charged half-unit-cell Sillen's phase $[(Bi_2O_2)(Cl)]^{1+}$ stacked upon a 1− charged half-unit-cell of an Aurivillius phase $[(Bi_2O_2)(NbO_4)]^{1-}$ (Fig. 3A). The c axial length is expected to be equal to the sum of the c axes of the half cells; in this case 6.5 Å + 8.2 Å = 14.7 Å. For the next members of the series perovskitic layers with increasing n may be substituted for the single layer. The conceptual structures of the $n = 2$ and $n = 3$ materials are shown in Figs. 3B and 3C. Again c axis lengths should be equal to the sums of the corresponding half cells, i.e., for $n = 2$, $c_0 = 6.5$ Å + 12.8 Å = 19.3 Å and for $n = 3$, $c_0 = 6.5$ Å + 16.4 Å = 22.9 Å.

Substitution on metal atom sites should be possible without altering these structures as long as a concomitant change in a

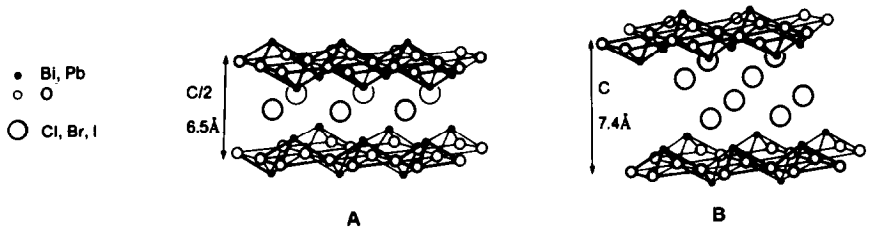

FIG. 2. Structures of Sillen's phases: (A) $PbBiO_2Cl$, (B) BiOCl.

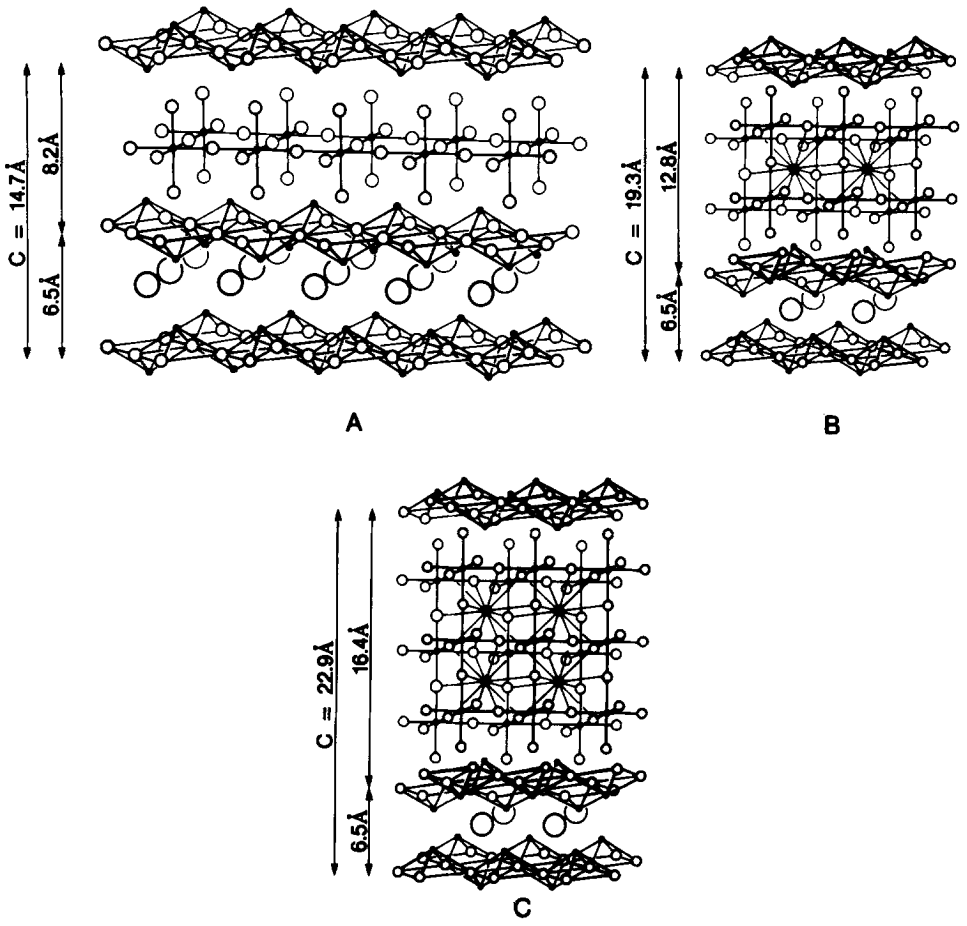

FIG. 3. Ideal structures of a mixed Aurivillius–Sillen system: (A) $n = 1$, (B) $n = 2$, (C) $n = 3$. Note commonality of $[Bi_2O_2]$ layers.

second atom is made to preserve electroneutiality. Thus, for the $n = 1$ material if one Bi is replaced by Pb, then Nb must be replaced by a hexavalent metal like W to produce $PbBi_3WO_8Cl$.

We report here the synthesis of several members of this new series and the refined crystal structures of two $n = 1$ materials Bi_4NbO_8Cl and $PbBi_3WO_8Cl$. Henceforth, we shall refer to the series by the achronym Bipox, a short form of bismuth perovskite oxyhalides.

Experimental

Polycrystalline Bipox samples were prepared by heating the appropriate oxides and oxyhalides, listed in Table I, to the given temperatures in sealed platinum tubes. The sintered materials were removed from the tube, ground in an agate mortar, and then refired at the same temperature in the same tube. As the size of the perovskitic layer increased it was necessary to slow cool the samples so that a homogeneous product was obtained. Although the melting points of the materials are low, single crystals could not be grown by the Czochralski technique due to the high volatility of the halides present in the melt. Slow cooling the melts in platinum tubes was also unsuc-

TABLE I

PREPARATIVE DETAILS FOR BISMUTH PEROVSKITE OXYHALIDE SYNTHESIS

	Reactants	Products	Temperature (°C)	Soak duration (hr)	Container	Comments
1.	3/2 Bi_2O_3 + 1BiOCl + 1/2 Nb_2O_5	Bi_4NbO_8Cl	950	3	Pt tube	Powder
2.	3/2 Bi_2O_3 + 1BiOBr + 1/2 Nb_2O_5	Bi_4NbO_8Br	900	3	Pt tube	Powder
3.	3/2 Bi_2O_3 + 1BiOCl + 1/2 Ta_2O_5	Bi_4TaO_8Cl	1000	3	Pt tube	Powder
4.	3/2 Bi_2O_3 + 1BiOCl + 1/2 TiO_2 + 1/2 WO_2	$Bi_4Ti_{0.5}W_{0.5}O_8Cl$	900	2	Pt tube	Powder
5.	2 Bi_2O_3 + 1BiOCl + 2TiO_2	$Bi_4Ti_3O_{12}$ + ?	950	3	Pt tube	Tube attack
6.	2Bi_2O_3 + 1BiOCl + 2ZrO_2	$Bi_5Zr_2O_{11}Cl$	1000	3	Pt tube	Powder
7.	5/2 Bi_2O_3 + 1BiOCl + 2TiO_2 + 1/2 Fe_2O_3	$Bi_6Ti_2FeO_{14}Cl$	900	3	Pt tube	Powder
8.	3Bi_2O_3 + 1BiOCl + 2TiO_2 + 1Fe_2O_3	$Bi_7Ti_2Fe_2O_{17}Cl$	900	3	Pt tube	Powder
9.	7/2 Bi_2O_3 + 1BiOCl + 2TiO_2 + 3/2 Fe_2O_3	$Bi_8Ti_2Fe_2O_{20}Cl$	875	4	Pt tube	Slow cooling necessary
10.	4Bi_2O_3 + 1BiOCl + 2TiO_2 + 2Fe_2O_3	$Bi_9Ti_2Fe_7O_{23}Cl$	850	4	Pt tube	
11.	9/2 Bi_2O_3 + 1BiOCl + 2TiO_2 + 5/2 Fe_2O_3	$Bi_{10}Ti_2Fe_5O_{26}Cl$	850	4	Pt tube	
12.	5Bi_2O_3 + 1BiOCl + 2TiO_2 + 3Fe_2O_3	$Bi_{11}Ti_2Fe_6O_{29}Cl$	825	4	Pt tube	
13.	11/2 Bi_2O_3 + 1BiOCl + 2TiO_2 + 3Fe_2O_3	$Bi_{12}Ti_2Fe_7O_{32}Cl$	825	4	Pt tube	
14.	6Bi_2O_3 + 1BiOCl + 2TiO_2 + 4Fe_2O_3	$Bi_{13}Ti_2Fe_8O_{35}Cl$	800	6	Pt tube	
15.	13/2 Bi_2O_3 + 1BiOCl + 2TiO_2 + 8/2 Fe_2O_3	$Bi_{14}Ti_2Fe_9O_{38}Cl$	800	12	Pt tube	
16.	1PbO + 1BiOCl + 1Bi_2O_3 + 1WO_3	$PbBi_3WO_8Cl$	900	2	Pt tube	Powder
17.	5/2 Bi_2O_3 + 1BiOCl + 1/2 Nb_2O_5 + 1WO_3	$Bi_6NbWO_{14}Cl$	950	4	Pt tube	Powder
18.	3PbO + BiOCl + 2Bi_2O_3 + 2Nb_2O_5	$Bi_5Pb_3Nb_4O_{20}Cl$	900	2	Pt tube	Powder
19.	1PbO + 2BiOCl + 1/2 Bi_2O_3 + 1/2 Re_2O_7	$Bi_3PbReO_8Cl_2$	750	12	Pt tube	Powder
20.	2BiOCl + 3PbO + 2WO_3	$Pb_3Bi_2W_2O_{11}Cl_2$	750	6	Pt tube	Powder
21.	Presintered Bi_4NbO_8Cl	Single-crystal Bi_4NbO_8Cl	1150	5	Al crucible	1 kg charge sealed in fused silica
22.	Presintered $PbBi_3WO_8Cl$	Single-crystal $PbBi_3WO_8Cl$	1000; slow cooled 5°C/hr	5	Al crucible	

cessful since the melts slowly attack Pt metal. Single crystals of $PbBi_3WO_8Cl$ were finally prepared by loading 1.0 kg of presintered material into an alumina crucible which was then sealed into an evacuated silica tube. The tube was heated to 1000°C, soaked for 5 hr, and then cooled at 10°C/hr to room temperature. The tube was opened and the crystalline mass separated mechanically from the alumina crucible. Single crystals of Bi_4NbO_8Cl were obtained using the same technique with a soak temperature of 1150°C.

X-Ray powder diffraction patterns were recorded on a Rigaku $\theta - \theta$ automatic diffractometer using normal ($\frac{1}{2}$°2θ/min) scan rates with pure Si (a_0 = 5.43088) as the calibrating standard. Refinement of lattice constants was done via least squares fitting of the high-angle reflections on a local computer program.

Single-crystal X-ray diffraction data were collected on a Nicolet P3F four-circle diffractometer using monochromatic Mo K_α radiation. For $PbBi_3WO_8Cl$ a full sphere of reflections with $3° \leq 2\theta \leq 55°$ were measured using a minimum 2θ scan speed of 1.0°/min and a maximum of 10°/min. Due to severe absorption of X-rays by the heavy atoms in the crystal an empirical absorption correction was applied to the data. Least squares fitting of the ψ scans made on 7 reflections produced minimum and maximum transmissions of 0.005 and 0.400. A half-sphere of reflections with $3° \leq 2\theta \leq 60°$ were recorded for Bi_4NbO_8Cl with scan speeds between 3° and 15°2θ/min. Again an empirical absorption correction based on 5 reflections was applied to the data yielding minimum and maximum transmission values of 0.003 and 0.49. Structure refinement was performed with the Nicolet structure program SHELXTL implemented on a Data General Eclipse computer.

Results and Discussion

Ceramic preparations produced polycrystalline materials ranging in color from yellow for Bi_4NbO_8Cl to brown for Fe-containing samples. No loss of material was detected by weight analysis for sealed tube synthesis with the exception of $Bi_5Ti_2O_{11}Cl$ charges. In these weight losses and Pt tube attack was always observed.

Microscopic examination of the polycrystalline masses indicated that all of the Bipox materials crystallize as rectangular platelets with aspect ratios of 50 to 100.

Powder diffraction patterns for these materials define tetragonal unit cells with the dimensions listed in Table II. Preferential orientation of the samples and subsequent high diffraction intensity for 00*l* reflections indicates that the axis normal to the crystalline plate faces was the unique tetragonal *c* axis.

TABLE II

TETRAGONAL (OR PSEUDOTETRAGONAL) LATTICE PARAMETERS OF BISMUTH PEROVSKITE OXYHALIDES

	Material		a_0 (Å)	× c_0 (Å)
1.	Bi_4NbO_8Cl	orth	5.493 × 5.496	× 28.75
2.	$PbBi_3WO_8Cl$		3.894	× 14.35
3.	Bi_4NbO_8Br		3.861	× 14.58[a]
4.	Bi_4TaO_8Cl		3.882	× 14.43[a]
5.	$Bi_5Zr_2O_{11}Cl$		3.846	× 17.90
6.	$Bi_6Ti_2FeO_{14}Cl$		3.890	× 22.11
7.	$Bi_7Ti_2Fe_2O_{17}Cl$		3.900	× 26.26
8.	$Bi_8Ti_2Fe_3O_{20}Cl$		3.909	× 30.31
9.	$Bi_9Ti_2Fe_4O_{23}Cl$		3.910	× 34.09
10.	$Bi_{10}Ti_2Fe_5O_{26}Cl$		3.912	× 38.07
11.	$Bi_{11}Ti_2Fe_6O_{29}Cl$		3.911	× 42.11
12.	$Bi_{12}Ti_2Fe_7O_{32}Cl$		3.913	× 45.91
13.	$Bi_{13}Ti_2Fe_8O_{35}Cl$		3.912	× 49.88
14.	$Bi_{14}Ti_2Fe_9O_{38}Cl$		3.913	× 54.15
15.	$Bi_4Ti_{0.5}W_{0.5}O_8Cl$		3.856	× 14.23
16.	$PbBi_3ReO_8Cl_2$		3.94	× 30.21[a]
17.	$Bi_2Pb_3W_2O_{11}Cl_2$		3.95	× 39.6[a]
18.	$Bi_6NbWO_{14}Cl$		3.85	× 45.4
19.	$Bi_5Pb_3Nb_4O_{20}Cl$		3.921	× 53.81

[a] Probable true symmetry is orthorhombic.

n = 1 Structures

Since $PbBi_3WO_8Cl$ and Bi_4NbO_8Cl crystals were the most facile to prepare and since these compounds represented the simplest members of this structural series, they were selected for single-crystal structure determination.

Bi_4NbO_8Cl

A flat single crystal was selected from a mass of twins by microscopic inspection between crossed polaroids. Single-crystal precession photos and analyses of systematic reflections established the space group to be orthorhombic $P2_1cn$ (a nonstandard setting of S.G. #33) with $a = 5.493 \pm 0.002$, $b = 5.496 \pm 0.002$, and $c = 28.75 \pm 0.01$. 3461 reflections were collected and merged into 920 unique independent reflections. Initially, positions of the heavy atoms were established with a Patterson map and the light atoms located in the later stages of re-

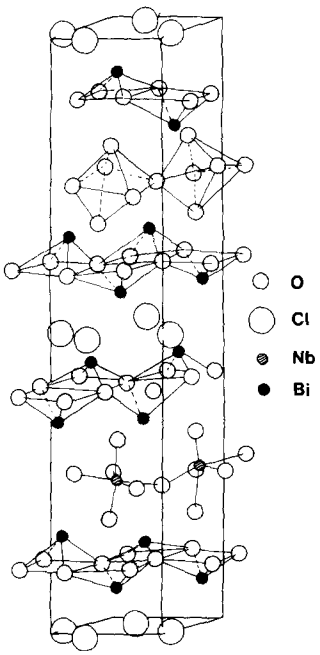

FIG. 4. The structure of Bi_4NbO_8Cl, Nb omitted in upper half of cell.

TABLE III

ATOMIC POSITIONS AND THERMAL PARAMETERS FOR Bi_4NbO_8Cl

Atom	x/A	y/B	z/C	U_{11}	U_{22}	U_{33}	U_{23}	U_{13}	U_{12}	U_{equiv}
Nb1	0.02913	0.24772	0.24906	0.0099	0.0001	0.0070	0.0000	0.0000	0.0000	0.0057
	0.00219	0.00086	0.00048	0.0028	0.0022	0.0027	0.0000	0.0000	0.0000	0.0015
Bi1	0.00000	0.81123	0.15737	0.0001	0.0168	0.0125	0.0000	0.0000	0.0000	0.0098
	0.00000	0.00062	0.00021	0.0010	0.0015	0.0022	0.0000	0.0000	0.0000	0.0010
Bi2	0.02912	0.25686	0.43242	0.0127	0.0001	0.0006	0.0000	0.0000	0.0000	0.0044
	0.00155	0.00058	0.00014	0.0033	0.0011	0.0018	0.0000	0.0000	0.0000	0.0013
Bi3	0.03844	0.78193	0.34299	0.0677	0.0222	0.0084	−0.0052	−0.0019	−0.0223	0.0328
	0.00172	0.00082	0.00024	0.0091	0.0020	0.0027	0.0017	0.0044	0.0047	0.0032
Bi4	0.04219	0.25618	0.06749	0.0103	0.0159	0.0159	0.0010	0.0002	−0.0072	0.0140
	0.00137	0.00089	0.00019	0.0033	0.0016	0.0028	0.0012	0.0014	0.0013	0.0015
Cl1	0.53187	0.21987	−0.00127	0.0210	0.0001	0.0141	0.0000	0.0000	0.0000	0.0017
	0.00585	0.00400	0.00092	0.0100	0.0112	0.0092	0.0000	0.0000	0.0000	0.0059
O1	0.74618	0.51263	0.39820	0.0001						
	0.01308	0.01040	0.00250	0.0113						
O2	0.32318	0.47417	0.40003	0.0001						
	0.01078	0.01131	0.00291	0.0132						
O3	0.82292	−0.01519	0.38348	0.0001						
	0.01007	0.01031	0.00258	0.0122						
O4	0.27806	0.00755	0.38873	0.0001						
	0.01098	0.01036	0.00281	0.0121						
O5	0.42655	0.71018	0.32318	0.0001						
	0.01132	0.01021	0.00215	0.0112						
O6	0.56653	0.65784	0.19301	0.0044						
	0.01214	0.00972	0.00253	0.0117						
O7	0.26993	−0.03809	0.24098	0.0005						
	0.01166	0.01089	0.00190	0.0109						
O8	0.07240	−0.10038	0.25911	0.0001						
	0.01030	0.00978	0.00206	0.0111						

finement by difference Fourier maps. Reiterative refinement of 86 independent parameters where the metal atoms were anisotropic the oxygens isotropic converged to a final R value of 9.5% with R_w = 15.0%. Electron density residuals at this point were located on the Bi atoms.

The atomic positions and isotropic thermal parameters for Bi_4NbO_8Cl are listed in Table III. Interatomic distances and angles are given in Table IV. The resulting structure is illustrated in Fig. 4 and can be seen to be a distorted variant of the ideal structure shown in Fig. 3A. The unit cell consists of 4 $[Bi_2O_2]$, 2 $[NbO_4]$, and 2 [Cl] layers. The layers are oriented normal to the c axis and have the sequence $[Bi_2O_2][NbO_4]$ $[Bi_2O_2][Cl][Bi_2O_2][NbO_4][Bi_2O_2][Cl]$. Whereas the [Cl] and $[Bi_2O_2]$ layers exhibit nearly coplanar atoms normal to c_0, the $[NbO_4]$ layers are composed of distorted octahedra which are canted with respect to one another. It is this canting which causes the observed c axis to be twice that of the ideal structure. Local environments of the metal atoms are shown in Figs. 5a–c and are similar to those seen in the Aurivillus and Sillen's phases.

$PbBi_3WO_8Cl$

A crystal of $PbBi_3WO_8Cl$ was selected by microscopic examination in polarized light. It too exhibited a flat rectangular plate morphology with dimension 0.11 × 0.18 × 0.05

TABLE IV

Bond	Length (Å)	Bond	Length (Å)
Nb–O5	2.14(7)	Bi1–O1	2.378(7)
–O6	1.72(7)	–O2	2.11(7)
–O7	2.11(6)	–O3	2.78(7)
–O8	2.10(5)	–O4	2.465(8)
–O7A	1.83(6)	–O5B	2.30(8)
–O8A	2.08(5)	–O5C	3.37(8)
		–O6A	2.26(7)
		–O6B	3.89(8)
Bi2–Cl	3.16(8)	Bi3–O1	2.46(8)
–ClA	3.51(8)	–O2	2.68(8)
–ClB	3.34(8)	–O3	1.90(5)
–ClC	3.45(8)	–O4	2.08(6)
–O1	2.32(7)	–O5	2.11(6)
–O2	2.19(6)	–O5A	3.07(7)
–O3	2.28(7)	–O6	3.29(8)
–O4	2.29(7)	–O6A	2.15(6)
Bi4–Cl	3.46(8)		
–ClA	3.29(7)		
–ClB	3.29(7)		
–ClC	3.16(8)		
–O1	2.04(6)		
–O2	2.15(6)		
–O3	2.43(6)		
–O4	2.34(6)		

Nb	O5–Nb–O6	157.2	O6–N6–O7	79.5	O7–Nb–O7A	175.2
	O5–Nb–O7	87.1	O6–Nb–O8	72.2	O7–Nb–O8A	70.8
	O5–Nb–O8	85.8	O6–Nb–O7A	98.1	O8–Nb–O7A	106.4
	O5–Nb–O7A	93.8	O6–Nb–O8A	94.2	O8–Nb–O8A	139.2
	O5–Nb–O8A	98.7	O7–Nb–O8	68.9	O7–Nb–O8A	113.6
Bi1	O1–Bi1–O2	62.4	O2–Bi1–O3	103.2	O3–Bi1–O5	146.0
	O1–Bi1–O3	68.7	O2–Bi1–O4	68.6	O3–Bi1–O5A	61.0
	O1–Bi1–O4	103.7	O2–Bi1–O4	72.9	O3–Bi1–O6	117.8
	O1–Bi1–O5	79.5	O2–Bi1–O5A	119.3	O3–Bi1–O6A	51.1
	O1–Bi1–O5A	129.6	O2–Bi1–O6	98.0	O4–Bi1–O5	133.8
	O1–Bi1–O6	110.5	O2–Bi1–O6A	136.8	O4–Bi1–O5A	50.6
	O1–Bi1–O6A	75.0	O3–Bi1–O4	69.5	O4–Bi1–O6	65.7
	O4–Bi1–O6A	117.5	O5–Bi1–O6A	107.9	O6–Bi1–O6A	124.2
	O5–Bi1–O5A	150.8	O5A–Bi1–O6	57.5		
	O5–Bi1–O6	95.9	O5A–Bi1–O6A	81.8		
Bi2	Cl1–Bi2–Cl1A	110.8	ClA–Bi2–O1	138.2	ClC–Bi2–O1	72.4
	Cl1–Bi2–Cl1B	68.0	ClA–Bi2–O2	134.1	Cl1C–Bi2–O2	143.3
	Cl1–Bi2–Cl1C	66.6	Cl1A–Bi2–O3	77.0	Cl1C–Bi2–O3	88.6
	Cl1–Bi2–O1	75.0	Cl1A–Bi2–O4	77.6	Cl1C–Bi2–O4	144.3
	Cl1–Bi2–O2	79.1	Cl1B–Bi2–Cl1C	108.0	O1–Bi2–O2	87.5
	Cl1–Bi2–O3	149.0	Cl1B–Bi2–O1	139.3	O1–Bi2–O3	79.0
	Cl1–Bi2–O4	145.4	Cl1B–Bi2–O2	68.1	O1–Bi2–O4	121.0
	Cl1A–Bi2–Cl1B	74.6	Cl1B–Bi2–O3	140.2	O2–Bi2–O3	117.9
	Cl1A–Bi2–Cl1C	73.3	Cl1B–Bi2–O4	83.2	O2–Bi2–O4	72.4
					O3–Bi2–O4	64.7

TABLE IV—*Continued*

Bi3	O1–Bi3–O2	67.07	O2–Bi3–O4	64.0	O4–Bi3–O5	73.5
	O1–Bi3–O3	66.4	O2–Bi3–O5A	124.7	O4–Bi3–O5A	137.1
	O1–Bi3–O4	102.4	O2–Bi3–O6	67.5	O4–Bi3–O6	130.8
	O1–Bi3–O5	127.8	O2–Bi3–O6A	137.9	O4–Bi3–O6A	78.8
	O1–Bi3–O5A	59.5	O3–Bi3–O4	67.5	O5–Bi3–O5A	149.2
	O1–Bi3–O6	73.4	O3–Bi3–O5	141.1	O5–Bi3–O6	72.2
	O1–Bi3–O6A	145.6	O3–Bi3–O5A	69.3	O5–Bi3–O6A	95.8
	O2–Bi3–O3	102.4	O3–Bi3–O6	139.0	O5A–Bi3–O6	84.1
	O2–Bi3–O4	66.2	O3–Bi3–O6A	82.6	O5A–Bi3–O6A	96.5
					O6–Bi3–O6A	132.4
Bi4	Cl1–Bi4–Cl1A	110.3	Cl1A–Bi4–O1	77.9	Cl1C–Bi4–O1	147.6
	Cl1–Bi4–Cl1B	65.1	Cl1A–Bi4–O2	130.1	Cl1C–Bi4–O2	142.7
	Cl1–Bi4–Cl1C	73.0	Cl1A–Bi4–O3	81.1	Cl1C–Bi4–O3	84.2
	Cl1–Bi4–O1	135.0	Cl1A–Bi4–O4	149.3	Cl1C–Bi4–O4	78.7
	Cl1–Bi4–O2	71.5	Cl1B–Bi4–Cl1	107.7	O1–Bi4–O2	69.6
	Cl1–Bi4–O3	150.9	Cl1B–Bi4–O1	79.2	O1–Bi4–O3	72.6
	Cl1–Bi4–O4	78.0	Cl1B–Bi4–O2	69.6	O1–Bi4–O4	118.0
	Cl1A–Bi4–Cl1B	67.8	Cl1B–Bi4–O3	141.7	O2–Bi4–O3	121.3
	Cl1A–Bi4–Cl1B	67.8	Cl1B–Bi4–O3	141.7	O2–Bi4–O3	121.3

TABLE V

ATOMIC POSITIONS AND THERMAL PARAMETERS FOR $PbBi_3WO_8Cl$

Atom	*x/A*	*y/B*	*z/C*	U_{11}	U_{22}	U_{33}	U_{23}	U_{13}	U_{12}	U_{equiv}
W	0.00000	0.00000	0.00000	0.0333	0.0333	0.0182	0.0000	0.0000	0.0000	0.0283
	0.00000	0.00000	0.00000	0.0008	0.0008	0.0011	0.0000	0.0000	0.0000	0.0005
Bi1[a]	0.50000	0.50000	0.19044	0.0399	0.0399	0.0345	0.0000	0.0000	0.0000	0.0381
	0.00000	0.00000	0.00042	0.0011	0.0011	0.0019	0.0000	0.0000	0.0000	0.0008
Bi2[a]	0.50000	0.50000	0.80745	0.0673	0.0673	0.0136	0.0000	0.0000	0.0000	0.0494
	0.00000	0.00000	0.00040	0.0013	0.0013	0.0017	0.0000	0.0000	0.0000	0.0009
Cl	0.50000	0.50000	0.50380	0.0477	0.0477	0.0085	0.0000	0.0000	0.0000	0.0346
	0.00000	0.00000	0.00141	0.0037	0.0037	0.0052	0.0000	0.0000	0.0000	0.0024
Bi3[a]	0.00000	0.00000	0.36512	0.0282	0.0282	0.0308	0.0000	0.0000	0.0000	0.0290
	0.00000	0.00000	0.00044	0.0009	0.0009	0.0018	0.0000	0.0000	0.0000	0.0007
Bi4[a]	0.00000	0.00000	0.63217	0.0270	0.0270	0.0161	0.0000	0.0000	0.0000	0.0234
	0.00000	0.00000	0.00039	0.0008	0.0008	0.0015	0.0000	0.0000	0.0000	0.0006
O1	0.00000	0.50000	0.28040	0.0226	0.0299	0.0183	0.0000	0.0000	0.0107	0.0236
	0.00000	0.00000	0.00233	0.0152	0.0173	0.0099	0.0000	0.0000	0.0153	0.0084
O2	0.00000	0.50000	0.70921	0.0425	0.0515	0.0211	0.0000	0.0000	−0.0002	0.0384
	0.00000	0.00000	0.00264	0.0190	0.0211	0.0111	0.0000	0.0000	0.0194	0.0102
O3	0.00000	0.50000	0.02216	0.0482	0.0250	0.0839	0.0000	0.0000	0.0085	0.0524
	0.00000	0.00000	0.00874	0.0179	0.0000	0.0812	0.0000	0.0000	0.0123	0.0277
O4	0.00000	0.00000	0.12632	0.2383	0.2383	0.0349	0.0000	0.0000	0.0000	0.1705
	0.00000	0.00000	0.00423	0.0496	0.0496	0.0222	0.0000	0.0000	0.0000	0.0245
O5	0.00000	0.00000	0.86809	0.1281	0.1281	0.0349	0.0000	0.0000	0.0000	0.0970
	0.00000	0.00000	0.00659	0.1684	0.1684	0.0222	0.0000	0.0000	0.0000	0.0797

[a] Bi refined as 3/4 Bi + 1/4 Pb by extrapolation of scattering factors.

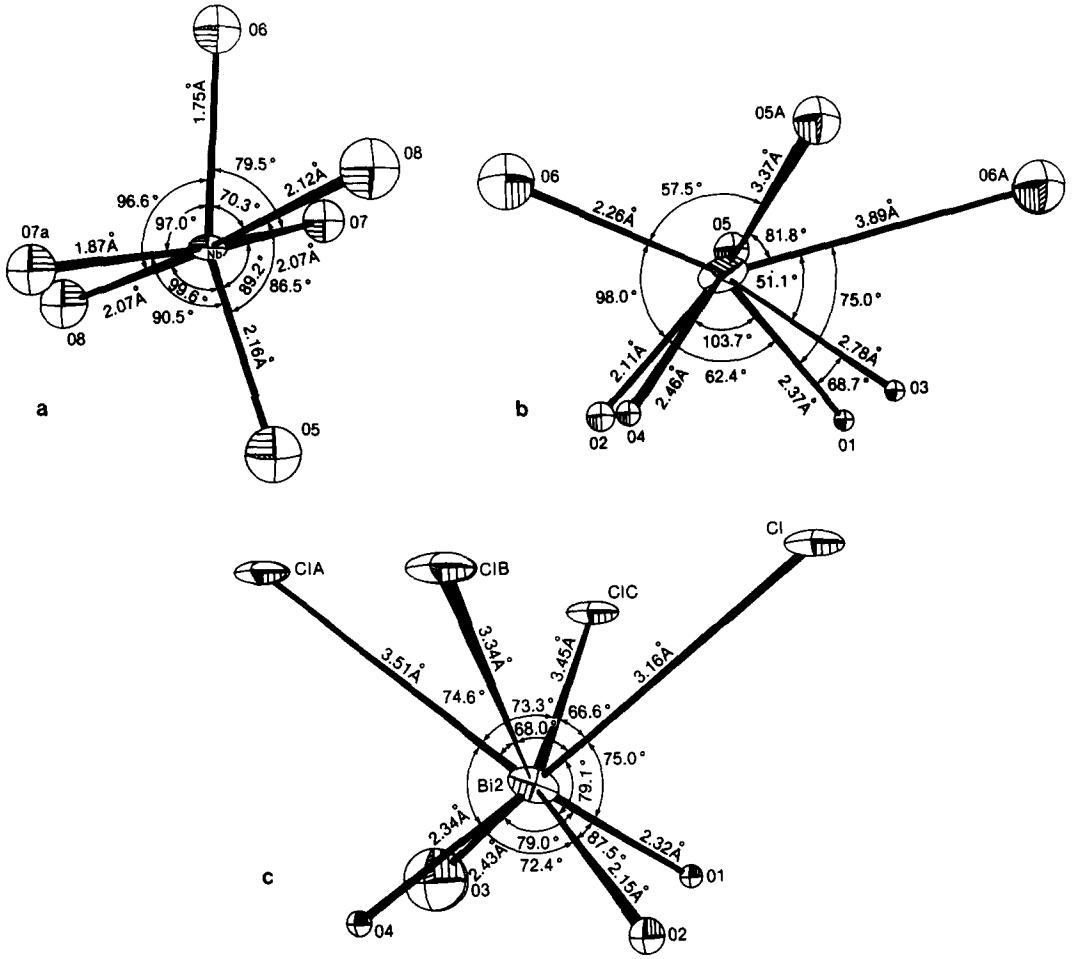

FIG. 5. Metal polyhedra in Bi_4NbO_8Cl: (a) Nb, (b) Bi1, (c) Bi2.

mm. Refinement of 20 centering reflections established the cell to be tetragonal with $a = 3.894 \pm 0.001$ Å and $c = 14.34 \pm 0.01$ Å. 2164 reflections were collected and merged into 390 independent reflections. No apparent extinction conditions were observed and subsequent refinements proved that the space group was in fact $P4$ (S.G. #75).

As before, a Patterson map was used to locate the heavy atoms and difference Fouriers used to locate the light atoms. Reiterative refinement of 37 independent parameters converged to a final R value of 5.3% with $R_w = 6.4\%$. The atomic positions and anisotropic thermal parameters for the final refinement are given in Table V. Bond lengths and angles are listed in Table VI and the structure is depicted in Fig. 6. It can be seen to have almost all of the essential features of the ideal $n = 1$ structure (Fig. 3A). The unit cell contains 2 $[Bi_2O_2]$, 1 $[MO_4]$, and 1 [Cl] layers. Unlike Bi_4NbO_8Cl this material has no canting of the $[MO_4]$ layer, and so does not have a doubled c axis. However, there is still a distortion of the WO_6 octahedra. This distortion is an elongation of one axial W–O bond followed by a movement of the W out of the plane of

TABLE VI

Bond length			
W–O3	1.97(2)	Bi1–O1	2.33(4)
W–O4	1.81(6)	Bi1–O4	2.90(10)
W–O5	1.89(9)		
Bi2–O2	2.40(4)	Bi3–Cl	3.40(3)
Bi2–O5	2.89(10)	Bi3–O1	2.29(4)
Bi4–Cl	3.31(3)		
Bi4–O2	2.24(4)		
Bond angles			
O3–W–O3A	88.5(.9)	O1–Bi–O1A	72.2(1.7)
O3–W–O4	80.7(3.6)	O1–Bi–O4	67.4(1.6)
O3–W–O5	99.3(3.6)	O4–Bi0–4A	84.2(1.7)
O4–W–O5	180(0)		
O2–Bi2–OO2A	69.9(1.8)	Cl–Bi3–ClA	69.9(.8)
O2–Bi2–O5	68.3(1.4)	Cl–Bi3–O1	79.9(1.0)
O5–Bi2–O5A	84.8(1.7)	O1–Bi3–O1A	73.7(1.4)
Cl–Bi4–ClA	72.0(.8)		
Cl–Bi4–O2	76.3(1.1)		
O2–Bi4–O2A	75.9(1.9)		

the 4 equitorial oxygens. This distortion is evident in Fig. 7a which shows the W environment.

Figures 7b and c show the Bi environments which are essentially undistorted with respect to those of the Aurivillius and Sillen's phases.

The structures of Bi_4NbO_8Cl and $PbBi_3WO_8Cl$ are remarkably similar to the ideal structure Fig. 3A predicted from the combination of the Aurivillius and Sillen half cells. The similarity of peak positions and intensities from powder data indicates that Bi_4TaO_8Cl, $Bi_4W_{0.5}Ti_{0.5}O_8Cl$, and Bi_4NbO_8Br crystallize with the Bi_4NbO_8Cl structure.

Results $n > 1$

Power diffraction patterns for the Bipox series define tetragonal unit cells with the dimensions listed in Table II. Efforts to resolve high-angle reflections were thwarted by large polarization when 2θ approaches 90°.

The materials corresponding to stoichiometries with higher values of n, exhibit similar a_0 dimensions with varying c axes (Table II). These c axes increase about 3.9 Å for every unit increase in n. By analogy to the Aurivillius phases this 3.9 Å increase corresponds to the addition of one metal–oxygen octahedral layer to that of the preceeding structure. Therefore, $Bi_5Zr_2O_{11}Cl$ should have a structure related to the one shown in Fig. 3B; $Bi_6Ti_2FeO_{14}Cl$ a structure related to that of Fig. 3C, etc. The largest c axis we have found is that of the $n = 11$ material $Bi_{14}Fe_9Ti_2O_{38}Cl$ whose ideal structure is depicted in Fig. 8. Whereas the orthorhombic deviation from tetragonal symmetry seen in Bi_4NbO_8Cl is possible in these materials it is likely that the canting and distortion of the metal–oxygen octahedra are not present with higher values of n. As n increases the structures become increasingly similar to perovskite with a greater degree of three-dimensional metal–oxygen–metal cross-linking. Such bonding inhibits the movement of the metal–oxygen octahedra and may preserve a tetragonal cell. Single-crystal structure determinations presently underway will show whether this is correct.

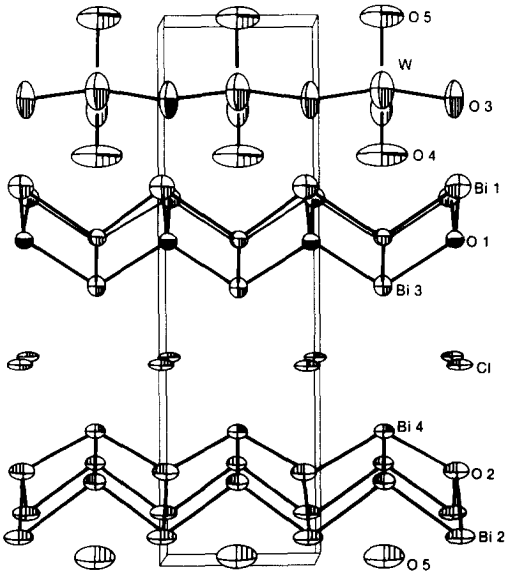

FIG. 6. The structure of $PbBi_3WO_8Cl$; cell outlined.

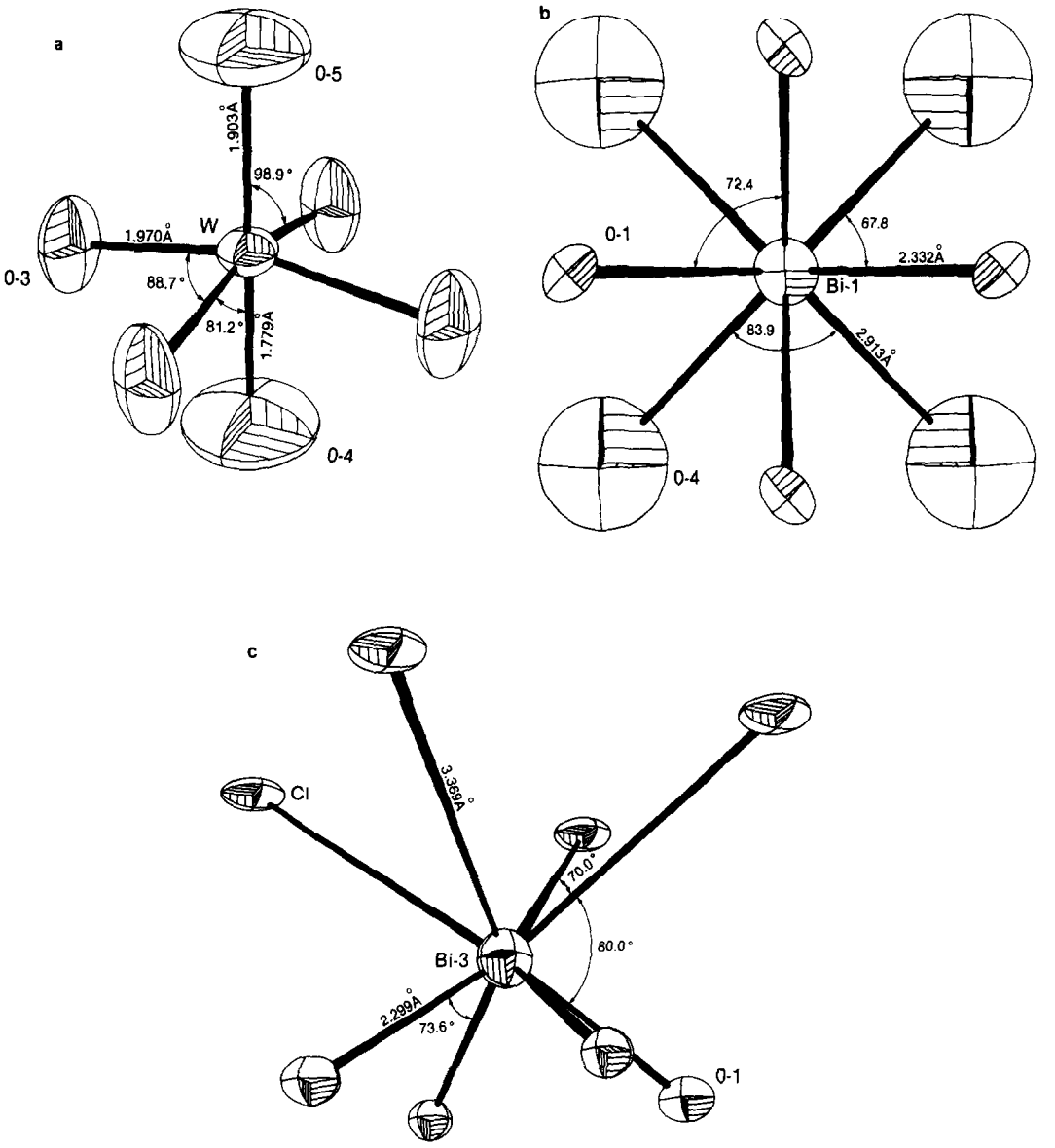

FIG. 7. Metal polyhedra in $PbBi_3WO_8Cl$: (a) W, (b) Bi1, (c) Bi3.

There are two other variations to the Bi-pox series in addition to a regular increase in n. One can conceive a structure in which two single and unique $[MO_4]$ layers exist with one [Cl] layers having the sequence

$$[[Bi_2O_2][MO_4][Bi_2O_2][MO_4][Bi_2O_2][Cl]] \cdot 2.$$

The expected c axis from a combination of 2 Aurivillius half-cells and one Sillen half-cell is 45 Å. Electroneutrality requires M to have a +5.5 charge. This is easily accomplished with $M = \frac{1}{2}Nb + \frac{1}{2}W$. Powder diffraction on $Bi_6NbWO_{14}Cl$ shows it to be tetragonal, $a_0 = 3.86$ Å, $c_0 = 45.4$ Å. Our theory predicts a structure related to that shown in Fig. 9. The same sequencing using

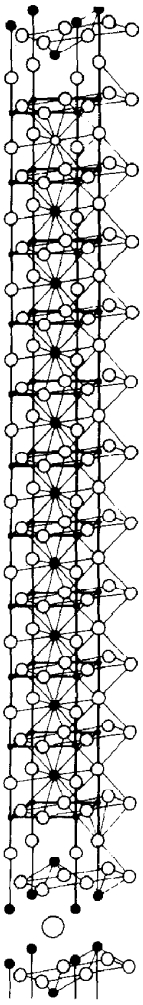

FIG. 8. Ideal structure of $Bi_{14}Fe_9Ti_2O_{38}Cl$.

double perovskite layers, $[AM_2O_7]$, is expected for $Pb_3Bi_5Nb_4O_{20}Cl$, tetragonal, $a_0 = 3.921$, $c_0 = 53.81$.

Finally one can envisage double halogen layers, such as those in BiOCl, present in a solid containing perovskitic layers as well. The sequence

$$[[Bi_2O_2][MO_4][Bi_2O_2][Cl][Cl]] \quad (C)$$

shown in Fig. 10, is exemplified by $PbBi_3ReO_8Cl_2$ with $c_0 = 30.2$ Å and $Pb_3Bi_2W_2O_{11}Cl_2$ with $c_0 = 39.6$ Å.

The Bipox phases represent a large variety of stoichiometries which would be difficult to represent on an elemental phase diagram. However, the entire series can be easily represented on a structural phase diagram. If we allow the endpoints of a ternary diagram to represent discrete structural layers, rather than stoichiometries, a ternary structural phase diagram, Fig. 11, results. Here any point describes a material having a specific ratio of perovskitic, halogen, or Bi_2O_2 layers. Note that two sides of the diagram represent those phases formed from Bi_2O_2 + halogens and Bi_2O_2 +

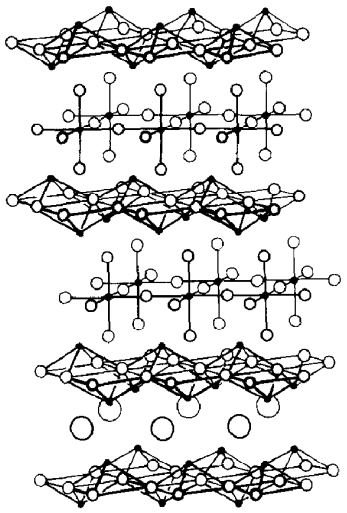

FIG. 9. The ideal structure of $Bi_6NbWO_{14}Cl$.

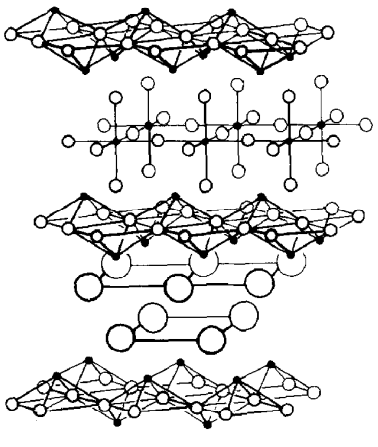

FIG. 10. The ideal structure of $PbBi_3ReO_8Cl_2$.

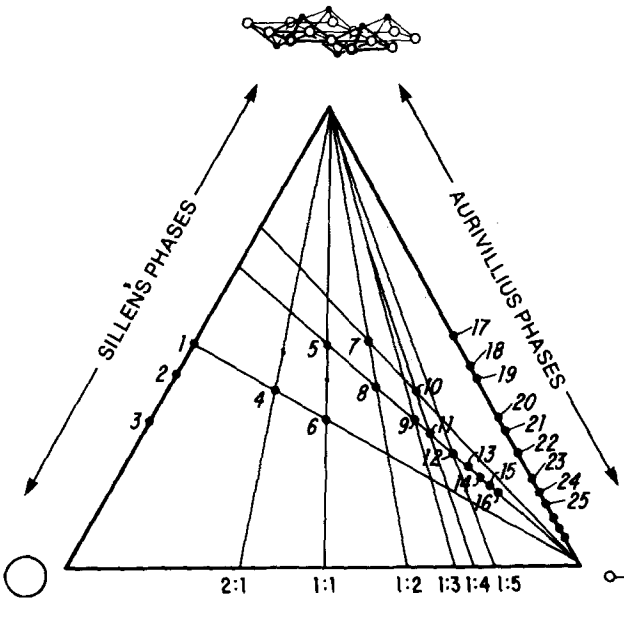

1 $PbBiO_2Cl$
2 $PbBi_3O_4Cl_3$
3 $BiOCl$
4 $Bi_4ReO_8Cl_2$
5 Bi_4NbO_8Cl
6 $Bi_2Pb_3W_2O_4Cl_2$
7 $Bi_6NbWO_{14}Cl$
8 $Bi_5Ti_2O_{11}Cl$
9 $Bi_6Ti_2FeO_{14}Cl$
10 $Bi_5PbNb_4O_{21}Cl$
11 $Bi_2Ti_2Fe_2O_{17}Cl$
12 $Bi_8Ti_2Fe_3O_{20}Cl$
13 $Bi_9Ti_2Fe_4O_{23}Cl$
14 $Bi_{10}Ti_2Fe_5O_{26}Cl$
15 $Bi_{11}Ti_2Fe_6O_{29}Cl$
16 $Bi_{12}Ti_2Fe_7O_{32}Cl$
17 Bi_2WO_6
18 $Bi_6Pb_3W_4O_{21}$
19 $Bi_5Nb_3O_{15}$
20 Bi_3TiNbO_9
21 $Bi_7Ti_4NbO_{21}$
22 $Bi_4Ti_3O_{12}$
23 $Bi_5Ti_3FeO_{15}$
24 $Bi_6Ti_3Fe_2O_{18}$
25 $Bi_7Ti_3Fe_3O_{21}$

FIG. 11. The terniary structural phase diagram for the Bipox series.

perovskites; that is the Sillen and Aurivillus phases. Tie lines culminating at the perovskitic endpoint represent the successive addition of one metal oxygen octahedral layer to the perovskitic layer. We believe that this diagram is by no means complete since the number of "gedanken" structures is infinite.

Conclusions

The structures of two single perovskite layer Bipox phases have been solved. The structures contain $[Bi_2O_2][MO_4]$ and [Cl] layers stacked along the c axis. Powder data on the remaining members of this series indicates that the thickness of the perovskitic layer can be increased in a regular manner, that more than one unique perovskitic layer per half cell may be incorporated into the structure, and that the halogen layers may be doubled.

Acknowledgments

It is a pleasure to acknowledge the synthetic help of W. B. Gibson, and crystallographic discussions with R. P. Goehner, M. F. Garbauskas, and J. Kasper.

References

1. B. AURIVILLIUS, *Arkiv. Kemi.*, **1**, 463, 1949.
2. L. SILLEN, *Z. Anorg. Allgem. Chem.*, **246**, 331, 1941.